NOTICE

CERTAIN DATA CONTAINED IN THIS DOCUMENT MAY BE DIFFICULT TO READ IN MICROFICHE PRODUCTS.

CONF-9206193--25

DE93 010174

Presented at the 1992 Advanced Accelerator Conference,
Port Jefferson, New York, June 14-20, 1992

EXPERIMENTAL GYROKLYSTRON RESEARCH AT THE UNIVERSITY OF MARYLAND FOR APPLICATION TO TEV LINEAR COLLIDERS

W. Lawson, V. L. Granatstein, B. Hogan, C.-V. Koc, P. E. Latham, W. Main, H. W. Matthews, G. S. Nusinovich, M. Reiser, C. D. Striffler, and S. Tantawi
Laboratory for Plasma Research and Department of Electrical Engineering
University of Maryland, College Park, MD 20742 USA

ABSTRACT

X-Band and K-Band gyroklystrons are being evaluated for possible application to future linear colliders. So far we have examined ten different two- and three-cavity configurations. We have achieved a maximum peak power of 27 MW in ~1 μs pulses at a gain of 36 dB and an efficiency exceeding 32%. The nominal parameters include a 430 kV, 150-200 A beam with an average perpendicular to parallel velocity ratio near one. In this paper, we detail our progress to date and describe our plans for future experiments that should culminate in amplifier outputs in excess of 100 MW in 1 μs pulses.

INTRODUCTION

An international effort is underway to develop amplifiers in the 10 - 30 GHz range with peak powers in excess of 100 MW for driving future multi-TeV electron positron colliders [1]. At the University of Maryland, we are concentrating on the use of gyrotron amplifiers to achieve the required parameters. At the time our project first got underway, the state-of-the-art power for gyroklystrons hovered near 50 kW due in part to limitations imposed by spurious oscillations [2]. As an intermediate step toward the 100+ MW goal, we constructed and tested a system which was designed to surpass the 50 kW level by a factor of 500 [3]. We have achieved our goal [4], in part by increasing the power capability of the standard gyrotron electron gun [5] and by developing improved microwave absorbers to enhance stability [6]. This paper represents a summary of experimental work to date [4], [7]-[12].

A schematic of our experimental facility is shown in Fig. 1. A 1 - 2 μs, 500 kV, 400 A line-type modulator provides the required beam power with a maximum repetition rate of 4 Hz. A resistive divider shunts half the current and provides the intermediate voltage required for the double-anode magnetron injection gun (MIG). The MIG was designed to have a space-charge limiting current of 400 A and an axial velocity spread under 7% at the nominal current of 160 A with an average perpendicular to parallel velocity ratio of $\alpha = 1.5$. However, because of instabilities we have not achieved an α greater than about 1.2. Considerable flexibility in the magnetic field profile is achieved by using four independent supplies to power eight water-cooled pancake coils. The design magnetic field is 0.047 T at the cathode and 0.565 T $\pm$ 0.005 T for 25 cm in the circuit region, but the magnetic field can be varied along the axis to optimize performance.

FG65-91ER40642

DISCLAIMER

An enlargement of the circuit region for the last two-cavity tube is shown in Fig. 2. The downtaper is lined with lossy dielectrics, which are indicated in black. The tapered ceramics are a non-porous mix of 20% SiC in 80% BeO. The other ceramics are made in-house from carbon-impregnated alumino-silicate. Most of the drift tube is also lined with lossy ceramics to suppress instabilities. A partially self-consistent code which includes realistic rf field profiles [13] and AC space-charge effects [14] is used to design the microwave circuit dimensions and predict amplifier performance. Power is injected from a 2 μs, 100 kW magnetron through a slit in the radial wall into the input cavity. Control over the quality factor (Q) in the input cavity is obtained from losses in a thin ceramic ring placed against the sidewall. The output cavity Q is predominantly due to diffractive losses from the cavity's output lip. The Q factors have spanned the range 125 - 500 in the various tubes, but the resonant frequencies have always been derived from an $m = 0$ TE mode at 9.85 GHz.

The output waveguide is shown in Fig. 1. A short 2° linear taper is followed by a non-linear taper which brings the waveguide radius to a value suitable for the copper beam dump. A cross-guide magnetic field at the end of the dump prevents high-energy electrons from traveling through the second non-linear taper and impinging on the five inch diameter half-wavelength BeO output window.

Two types of microwave diagnostics can be attached to the output waveguide. An anechoic chamber uses an open-ended piece of X-band waveguide as a receiving antenna to estimate output power and mode purity via far field measurements. The horn can be rotated by 90° and remotely swept transverse to the z-axis over one meter. The signal is split into several different size waveguides for instantaneous frequency estimates and is fed to an HP 8566B spectrum analyzer for time-averaged frequency resolution. Calibration measurements have been in good agreement with an uncertainty less than $\pm$ 1 dB. The second diagnostic involves an overmoded directional coupler and a liquid calorimeter. The coupler provides the microwave power envelope and gives an additional peak power estimate. The calorimeter consists of a methanol - water mixture flowing between two 17° conical pieces of polyethylene. Bench test measurements against a 20 W CW signal have given similar agreement for these diagnostics.

A total of six two-cavity and four three-cavity gyroklystron tubes have been tested. A summary of the main features of each tube is presented in Table 1. The table mainly denotes the features that were changed in going from one tube to the next. That is, the cavity Qs, the amount of loss in the various regions, and the output wall taper. In addition, the table displays the progression of the operating regime of the beam parameters. In Table 2, the main results from each tube are presented. These include the peak power, the peak efficiency, and the peak gain. The table also indicates the magnetic field profile employed and the factor that resulted in limiting the tube performance. In addition, the reference where more details can be obtained is given. A summary of the progress toward achieving high peak power is shown in Fig. 3. The saturated gain at each power level is also

indicated. In the next two sections we will detail the results displayed in Table 1 and 2 and Fig. 3.

EXPERIMENTAL RESULTS–TWO CAVITY CIRCUITS

The first two tubes were plagued by a multitude of instabilities, produced power levels below the state of the art, and had signal gains less than 0 dB. These results occurred at a beam voltage of 183 kV, a current of 55 A, and a velocity ratio of $\alpha \approx 0.45$. The instabilities could be grouped into four classes. Modes in the first class existed mainly in the output waveguide in frequency ranges where the window was a good reflector. These modes required good post-output cavity beam quality and were suppressed by amplifier operation. The second class existed in the output waveguide adjacent to the output cavity and required significant reflections from the first non-linear taper. Whole tube modes comprised the third class and had their energy mainly in the drift tube with reflections provided by the cavities. The final mode class involves instabilities in the downtaper.

Instabilities in classes 3 and 4 were the most troublesome and usually involved modes with one azimuthal variation. These modes can be controlled by the introduction of loss into the downtaper and drift tube. Figure 4a shows the total single pass attenuation of the TE_{11} mode through these regions in Tube 1 in the most troublesome frequency range. The downtaper had only a few thin lossy rings and very little attenuation. The drift tube consisted of alternating rings of copper and ceramic (1% SiC in 99% MgO) in nearly equal amounts. Though there were some highly absorptive resonances, there was a large frequency range with negligible loss. In contrast, Fig. 4b shows the TE_{11} attenuation for Tube 6. This attenuation was sufficient to allow operation at the parameters listed in the abstract.

Tube 3 incorporated a downtaper and drift tube with attenuations near the final values of Fig. 4b. This allowed significant beam power to be used for the first time and resulted in a one and a half order of magnitude increase in output power. The input and output cavity Qs were 175 and 145, respectively. In a flat magnetic field of 0.452 T, a peak power above 1.5 MW was produced at 9.866 GHz when the beam voltage was 305 kV and the current was 108 A. Parameter space for amplification was limited by a class 2 instability near the amplifier frequency. We determined that the mode was the TE_{121} operating near cutoff in a constant radius waveguide section immediately following the output cavity. This mode could not be suppressed by amplifier operation but was eliminated in Tubes 4 and beyond by introducing a linear wall taper after the output cavity lip. With this modification, Tube 4 produced peak powers near 2.7 MW with a 427 kV, 130 A beam in a constant magnetic field of 0.537 T. Maximum efficiencies of both Tubes 3 and 4 were approximately 5%.

The final order of magnitude increase in power was achieved with Tube 5, which had additional loss in the downtaper and a higher Q in the output cavity (224). The primary performance increase came not from the circuit modifications

Table 1: Features of each Tube.

Tube	$V_{0,max}$ kV	I_0 A	Output cavity α	Input cavity Q	Buncher cavity Q	Output cavity Q	Output taper slant	Downtaper	Preliminary drift space	Drift tube
1	185	< 55	< 0.45	175	—	160	0°	Metal/lossy flat rings of C/AL-Sil.	Metal/lossy flat rings of C/AL-Sil.	Cu/lossy flat rings of 1% SiC, 99% MgO
2	325	< 150	< 0.49	175	—	160	//	Added loss	Added loss	//
3	375	40-140	< 1.0	175	—	145	//	Covered gate value. Added loss plus lossy flat rings of 20% SiC, 80% BeO	Metal/lossy flat rings of 20% SiC, 80% BeO.	Cu and nonperiodic configuration of tapered lossy rings of 20% SiC 80% BeO
4	425	< 200	< 1.0	175	—	160	2°	//	//	//
5	440	<200	<1.0	214	—	224	//	Added loss and some tapered pieces	Added loss with all tapered pieces	//
6	440	<200	<1.0	500	—	224	//	Added loss	Added loss	Added loss
7	440	<225	.6-.7	250	270	200	2.2°	//	C/AL-Sil. everywhere flat	
8	440	<225	.7-.8	//	//	350	//	C/AL Sil.	//	//
9	440	<225	.7-.8	//	//	465 Long	> 2.2°	//	//	//
10	440	<225	.7-.8	//	//	700 TE_{012}	//	//	//	//

Table 2: Results of amplification studies for each Tube.

Tube (Ref)	Magnetic Field Configuration	Ouput Power - MW	Efficiency	Gain	Limiting Factor
1 (8)	Flat fields	$< P_{in}$	—	< 0 dB	Instabilities everywhere
2 (8)	//	—	—	—	//
3 (8)	// 0.452 T	1.5 MW [305 kV, 108 A]	5%	15-16 dB	Instability in region of output cavity/ waveguide
4 (8)	// 0.537 T	2.7 MW [427 kV, 130 A]	5%	19 dB	Instability in downtaper
5 (4)	Tapered fields: optimum 0.474 T in output cavity, 15% higher in input cavity	22 MW [425 kV, 150 A]	$\leq 32\%$	≤ 26.5 dB	//
6 (9)	//	24 MW [425 kV, 190 A]	$\leq 34\%$	≤ 34 dB	//
7 (10)	Tapered fields: strong & weak profiles, $\sim 20\%$ and $\sim 30\%$ tapers	23 MW [425 kV, 205 A]	$\leq 36\%$	≤ 31 dB	//
8 (10)	//	27 MW 20 MW 16 MW	32% 28% 37%	36 dB 50 dB 33	//
9 (12)	//	22 MW	$< 28\%$	< 44 dB	//
10 (12)	//	22 MW	$< 27\%$	< 32 dB	//

but rather from the introduction of magnetic field tapering. A careful search of parameter space showed that the optimal input cavity field was 0.545 T while the best output cavity performance occurred at 0.474 T. Figure 5 reveals the dependence of peak power on input cavity magnetic field when the output cavity field is fixed at the optimal value. The beam voltage and current were 425 kV and 150 A, respectively. The simulated velocity ratio was $\alpha \approx 0.98$ in the output cavity and varied adiabatically with the magnetic field. At the optimum level, $\alpha \approx 1.15$ at the center of the input cavity. The efficiency at the maximum was 31% and the gain exceeded 26 dB.

The input power was limited to 45 kW due to breakdown at the input window and the drive curve indicated that Tube 5 was not saturated. An increase in the input cavity Q to ~500 in Tube 6 allowed saturation to be examined. Theory predicted this Q to be 80% of the required start oscillation value and oscillations were in fact observed in the input cavity at some points. The optimal amplified power occurred with the same 15% field profile. Two distinct points were examined. The first was the maximum efficiency point, where 22 MW was produced at 9.871 GHz with an efficiency of 34% and a gain of 34 dB. The beam voltage and current were 425 kV and 150 A, respectively. Figure 6 shows the time dependence of the cathode voltage and output power as measured by a calibrated crystal detector. The second point had a maximum power level of 24 MW at 9.875 GHz for the same field profile and beam voltage but with a current of 190 A.

EXPERIMENTAL RESULTS-THREE CAVITY CIRCUITS

The three-cavity tubes had three distinct departures from the two-cavity designs. A schematic of the three-cavity circuit is shown in Fig. 7. The first departure, of course, was the introduction of the buncher cavity whose Q (~270) was defined solely by an alumino-silicate ring on the outer wall. Two metal rods with rounded ends provided remote-controlled tunability of 120 MHz by adjustment of their insertion length. The second change was to use exclusively alumino-silicate in the drift tubes (Tubes 7 and beyond) and downtaper (Tubes 8 and beyond). The TE_{11} attenuation was always superior to their non-porous counterparts, the TE_{01} attenuation was adequate for cavity isolation at 9.85 GHz, and no outgassing problems were observed. The third difference was to use a lossy dielectric on the radial wall of the input cavity and modify the coupling slit. Both input cavities performed well; no noticeable advantages of either design were discerned during the amplifier studies.

All of the three cavity tubes had at least two distinct operating regimes controlled by the magnetic field taper. Figure 8 shows the axial variation of the magnetic guide field for these two regimes. The tapers which optimize each of the operating regimes vary slightly from tube to tube, so we give the range of tapers used. The steep taper has a 30-32% decrease and a field of 0.458 T in the output cavity, and the weak taper has a decrease of 17-22% and a field of 0.453-0.490 T in the output cavity. The two regimes were also affected differently by increased load reflections.

The primary difference in Tubes 7 to 10 is in the geometry of the output cavities. Figure 9 shows the output cavity cross-section of each of the tubes. Tube 7 operated well at high input power, producing 23 MW at 27% efficiency and 31 dB gain. At low input power, instabilities limited operation to lower α, or lower beam power. This prevented operation at higher gain and high power. We also discovered that the tube produced higher power when operated with the calorimeter (2% reflection) as opposed to the anechoic chamber (< 0.1% reflection).

We suspected that the downtaper instabilities observed in Tube 7 were suppressed with higher input power and thus we significantly increased the attenuation in the downtaper in Tube 8. We also suspected that the enhanced operation with a more reflective load indicated that a higher Q in the output cavity was necessary. At our optimum beam power (425 kV and 205 A) Tube 7 was operating at 5% of start oscillation current in the output cavity so we also increased the output cavity Q from 200 (Tube 7) to 350 (Tube 8). With these changes Tube 8 achieved 50 dB saturated gain at 20 MW, and 36 dB at the high power point of 27 MW where the efficiency was 32%. The tube was able to operate stably with input power near one hundred watts.

Ongoing numerical modeling of this device which considers only cavity modes has shown efficiencies from 21% to 38% depending on how the beam loading affects the cavity Qs and the value of the pitch angle. The theoretical results [15] are not consistent with the beam α predicted by the gun code [16]. Concerned that some of the interaction was occurring after the output cavity we decided to increase the length of the output cavity. The cavity could be lengthened while keeping the same operating frequency, either by reducing the radius, Tube 9, or by going to the second axial harmonic, TE_{012}, Tube 10. We also included a probe in the radial wall of the output cavity in Tubes 9 and 10 to directly monitor the cavity interaction.

For Tube 9, the best power and gain occurred at the same operating point and were 22 MW and 44 dB. In the weak taper regime the uncalibrated probe signal was directly proportional to the measurement made in the anechoic chamber. This suggests that the weak taper corresponds to an interaction in the output cavity. The probe indicated that for a strong taper the interaction occurs somewhere else.

The output cavity in Tube 10 had the same radius as both Tube 7 and 8 and an output cavity lip thickness the same as Tube 8. The cavity length, which was almost twice that of Tube 7 and 8 was intended to operate in the TE_{012} mode. The long length of the cavity caused the TE_{011} and similar lower order modes with one axial variation to have high Q, and hence low start oscillation currents (< 10 A). To suppress these modes, a thin ring of lossy dielectric was placed on the axial mid-plane of the cavity. Cold tests showed that this ring did not affect the Q of the TE_{012} mode while substantially reducing the Q of all single axial variation modes. As for Tube 9, initial observations indicate that Tube 10 has two regimes of operation. In one regime the output power is mostly due to interaction after the output cavity and in the other regime there is strong interaction in the output

cavity. Tube 10 has a maximum output power of 22 MW.

To compare the operation of the four tubes, Fig. 10 shows plots of efficiency vs. beam current for each tube at the beam voltage of 425 kV. As expected from their similar designs, Tubes 7 and 8 gave similar operation. The increased Q in Tube 8 allows it to operate better in the current regime of 100-200 A. The efficiency of Tube 9 shows a strong dependence on beam current in the range of 150-200 A. Below 100 A, where large alphas could be achieved, the tube free-oscillated at the operating frequency. Tube 10, which had the longest output cavity, had significantly lower efficiency than Tubes 7 and 8.

FUTURE EXPERIMENTS

With the success of the intermediate experiments, we are now contemplating our approach to a 100+ MW device. The high power requirement places several constraints on the electron gun and the microwave circuit. To produce a higher power MIG, we must either increase the beam voltage, increase the peak electric field in the gun, enlarge the average beam radius, or decrease the applied magnetic field [17]. The new microwave circuit must continue to be stable to spurious modes, provide inter-cavity isolation, and dissipate a fair amount of average power. Our options will be explored by performing cold test studies, constructing and testing additional tubes with the existing beam parameters, and designing MIGs and microwave circuits for 300 - 400 MW beams.

Near term plans

While the low repetition rate of our facility doesn't allow an examination of the system's average power considerations, the only unique gyroklystron feature of potential concern is the power dissipated in the lossy ceramic of the penultimate cavity. We are initiating a study of the effects of temperature rise and means of cooling via a cold test mock-up of the buncher cavity. The available power in our 2.5 kW CW klystron is considerably higher than the current estimate of penultimate cavity energy deposition.

One way to lower magnetic field is to inject at the fundamental and extract at the second harmonic. We will test this concept by replacing the output cavity of Tube 6 with the 19.7 GHz TE_{02} cavity shown in Fig. 11. Several of the key dimensions are indicated in the figure. The small cavity radius insures that the TE_{01} cannot exist at 9.85 GHz. The adiabatic wall transitions are designed to minimize mode conversion to the TE_{01} at 19.7 GHz. A cold cavity design code indicates that the power flowing into the drift tube is 50 dB lower than the power extracted at the end of the system. Simulations of amplifier stability and operation have been performed assuming the nominal experimental beam parameters. The design quality factor of 780 exceeds the start oscillation requirement for magnetic fields above 0.545 T. Efficiencies of at least 25% have been predicted by the large signal code.

The output cavity has been constructed and cold tested. The measured parameters are f=19.64 GHz and Q=685. The existing non-linear tapers are inadequate in terms of TE_{01} - TE_{02} mode conversion, so new tapers with Dolphchebychev profiles and theoretical mode conversion under 45 dB have been designed and are being electroformed. Also under construction are a 60 dB overmoded TE_{02} directional coupler and mode converters from TE_{10} rectangular to TE_{01} circular and from TE_{01} to TE_{02} in circular waveguide.

Three additional experimental configurations are under consideration. The first is simply a shorter output cavity to be used if spurious oscillations in the output cavity become a problem. The only potential drawback is an increase in the 19.7 GHz TE_{01} mode content. A single short cavity filter before the output cavity can potentially increase isolation.

The other two approaches are aimed at improving efficiency. First, an inner conductor will be inserted into the second harmonic tube. The 2 mm radius will increase isolation between cavities. In the downtaper, the inner radius will be increased and lossy dielectrics will be added in an attempt to further suppress class 1 modes. Because of the electric field distribution of the TE_{11} mode, we anticipate a significant improvement in attenuation in the section closest to the gun. This should result in a higher attainable velocity ratio which the non-linear code predicts will translate into better efficiency.

If the velocity ratio cannot be improved, an alternative approach to higher efficiency and lower magnetic field is to operate at the fundamental with a large Doppler shift $k_z v_z$. We are currently designing a traveling wave output section (gyro-twistron) which would replace the output cavity of Tube 6. Though the design is not yet completed, initial indications are that efficiencies of 35% are possible with the existing experimental beam parameters.

Finally, two alternative concepts which could be tested on the existing facility are also being explored. A second harmonic output traveling wave section can be used to eliminate the backward TE_{01} component and insure isolation. The second approach is to use non-symmetric modes to enhance beam - microwave coupling at the second harmonic.

Long Term Plans

The approach to a 100+ MW system is dependent on the current and near term experiments and the selection of the optimal amplifier frequency. To conform to conventional modulator and emitter technology, we assume the new system's maximum beam voltage and cathode loading will be 500 kV and 8 A/cm^2, respectively. This implies that higher current, probably with a larger guiding center radius, gives the required approach to higher powers. As the guiding center is increased, one must either (1) use an extremely lossy lining (~15-20 dB per wavelength), (2) choose a mode with a higher cutoff, or (3) use a coaxial insert in order to maintain cavity isolation. Even if a material could be found that satisfies (1),

the required heat load would probably be prohibitive. Approach (2) would require suppression of the lowest radial mode with the same azimuthal index (m) as the operating mode or a large increase in m. Either approach would probably entail a new input cavity scheme. The third approach is viable provided that TE_{0n} modes are used.

We have considered MIG designs at 11.424 GHz and 19.7 GHz for fundamental and second harmonic devices with 300 MW beams in coaxial geometry. All designs appear feasible with the fundamental 19.7 GHz design being the most difficult. In the following paragraphs, we detail only a scenario for a second harmonic experiment at 11.424 GHz. Other scenarios are receiving similar scrutiny.

Table 3. Nominal system parameters – 100+ MW System.

Beam Voltage	500 kV
Beam Current	600 A
Velocity Ratio	1.5
Magnetic Field	3.28 kG
Input Cavity	
Length	2.30 cm
Q	70
Output Cavity	
Length	4.20 cm
Q	368
Drift Tube	
Length	18 cm
Inner Radius	1.6 cm
Outer Radius	3.9 cm

A schematic for a system that utilizes a 5.712 TE_{01} input cavity and a second harmonic TE_{02} output cavity is shown in Fig. 12. Tentative parameters for such a system are given in Table 3. The current will be supplied by doubling the number of PFNs in the modulator and decreasing the repetition rate. The longer magnetic field region required for the interaction will be achieved by adding two field coils. The same supplies can be used as the magnet power requirement is considerably reduced at the lower field. Scaling the current beam from 200 A to 600 A requires a three-fold increase in guiding center radius. The inner conductor will be supported at the end of the beam dump and will include lossy ceramics to enhance stability. The output cavity radius is selected to preclude fundamental TE_{01} operation but may have to be increased if spurious modes become a problem. Initial large-signal modeling has predicted efficiencies above 27%; we expect this value to increase significantly when the design is optimized.

A MIG which provides the required beam parameters is shown in Fig. 13. Its single anode configuration reduces its overall size and complexity and eliminates compensation problems associated with the resistive divider. Simulations are performed with the EGUN [16] code. The average cathode radius is 7.13 cm and

the magnetic field compression is 7.55 at $\alpha = 1.5$. The peak electric field is less than 90 kV/cm on the cathode and 30 kV/cm on the anode. The nominal current is only 26% of the space-charge limiting value. The simulated beam thickness allows only 1.1 mm clearance between the beam and the drift tube walls.

The emitter strip is slightly curved to reduce velocity spread with an average half-angle of 46°. The dependence of axial velocity spread on current is shown in Fig. 14 [18]. The magnetic field at the cathode is adjusted to maintain $\alpha = 1.5$. Near the design current, the beam is not fully mixed by the input cavity. This accounts for the difference in spread between the two cavities. The design can operate over an 800 A range with a velocity spread below 10% due to the laminar flow of electrons throughout much of the gun. This extended range will facilitate the study of high efficiency amplification in the 100+ MW regime.

ACKNOWLEDGMENT

This work was supported by the United States Department of Energy.

We wish to acknowledge the efforts of C. Bellamy, J. Cheng, O. Dajani, S. Demske, K. Lee, Q. Qian, M. Rimlinger and V. Specht.

REFERENCES

1. Proc. Int. Workshop on the Next Generation Collider, SLAC Report-335, Dec. 1988.

2. W. M. Bollen, et al., IEEE Trans. Plasma Sci. Vol. PS-13, p. 117 (1985).

3. K. R. Chu, et al., IEEE Trans. Plasma Sci. Vol. PS-13, p. 424 (1985).

4. W. Lawson, et al., Phys. Rev. Lett. Vol. 67, p. 520 (1991).

5. W. Lawson, et al., Int. J. Electron. Vol. 61, p. 969 (1986).

6. J. P. Calame and W. Lawson, IEEE Trans. Electron Dev. Vol. 38, p. 1538 (1991).

7. W. Lawson et al., AIP Conference Proceedings 193, Advanced Accelerator Concepts, Lake Arrowhead, CA, 1989, Editor, Chan Joshi, p. 274.

8. J. P. Calame, et al., J. Appl. Phys. Vol. 70, p. 2123 (1991).

9. W. Lawson, et al., IEEE Trans. Plasma Science Vol. 20, No. 3 (1992).

10. S. Tantawi, et al., IEEE Trans. Plasma Science, Vol. 20, No. 3 (1992).

11. W. Lawson, et al., Proceedings of the Beams '92 Conference, Washington, DC, May 1992.

12. W. Main, et al., Proceedings of the Beams '92 Conference, Washington, DC, May 1992.

13. J. Neilson, et al., IEEE Trans. Microwave Theory Tech. Vol. MTT-37, p. 1165 (1989).

14. P. E. Latham, IEEE Trans. Plasma Sci. Vol. 18, p.273 (1990).

15. P. E. Latham, et al., Proceedings of the Beams '92 Conference, Washington, DC, May 1992.

16. W. B. Herrmannsfeldt, SLAC Report-226, Nov. 1979.

17. W. Lawson, IEEE Trans. Plasma Sci. Vol. 16, p. 290 (1988).
18. W. Lawson and V. Specht, submitted to IEEE Trans. Electron Dev., May 1992.

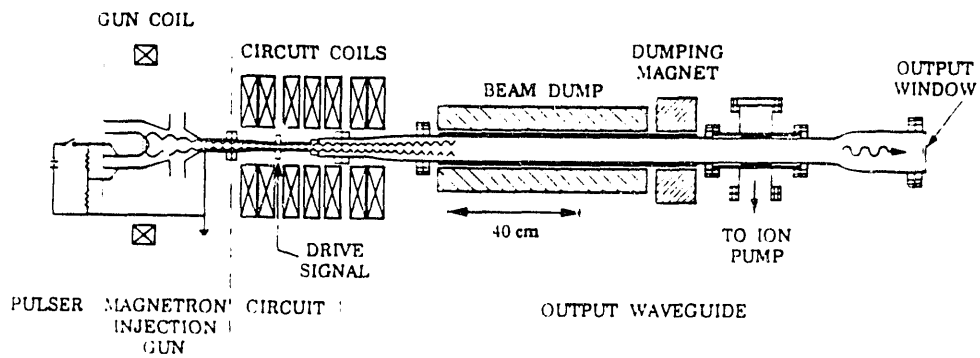

Figure 1. A schematic view of the gyroklystron experimental facility.

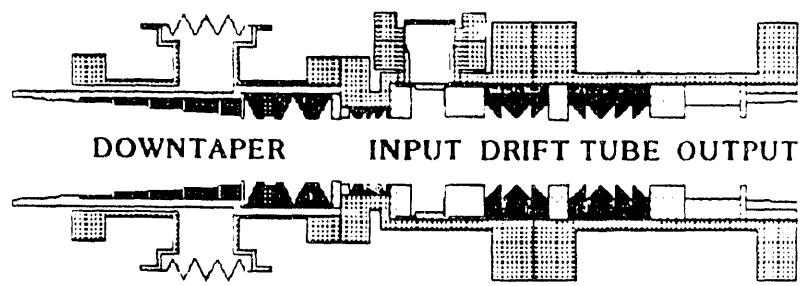

Figure 2. The two-cavity microwave circuit configuration.

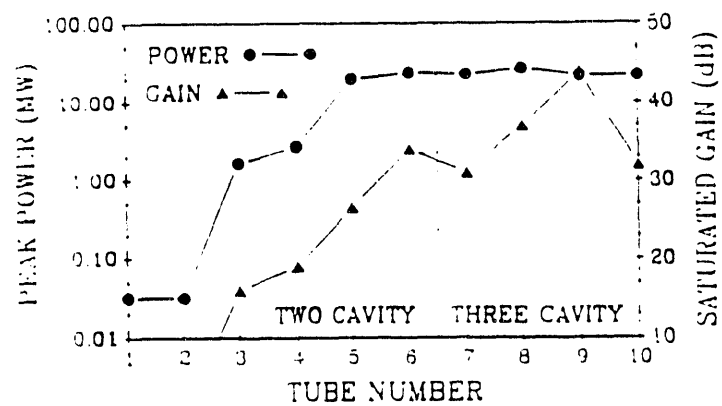

Figure 3. Summary of tube peak power performance.

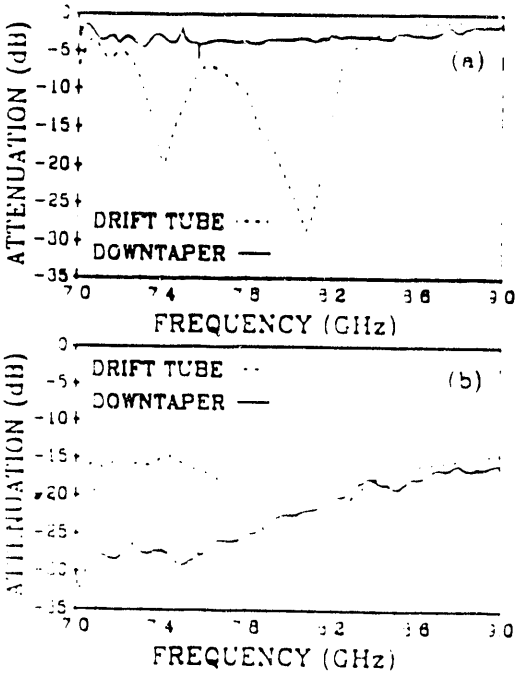

Figure 4. TE_{11} attenuation vs. frequency in the downtaper and drift tube regions: (a) for Tube 1 and (b) for Tube 6.

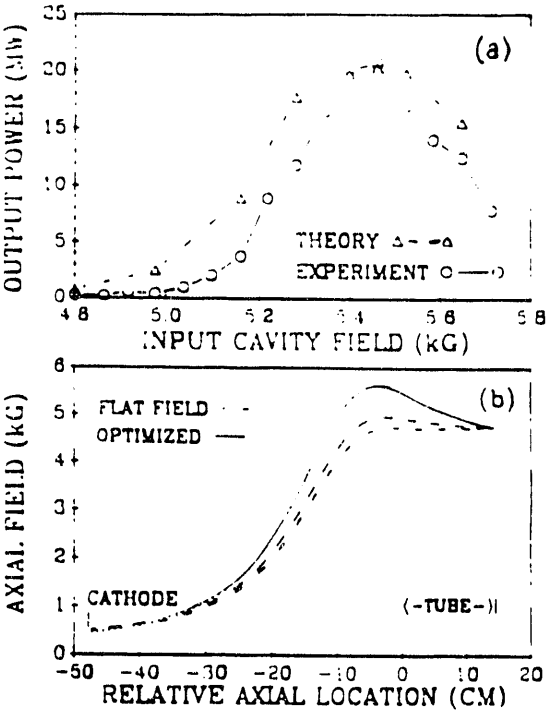

Figure 5. (a) Peak measured and theoretical output power vs. input cavity magnetic field. (b) axial field profile.

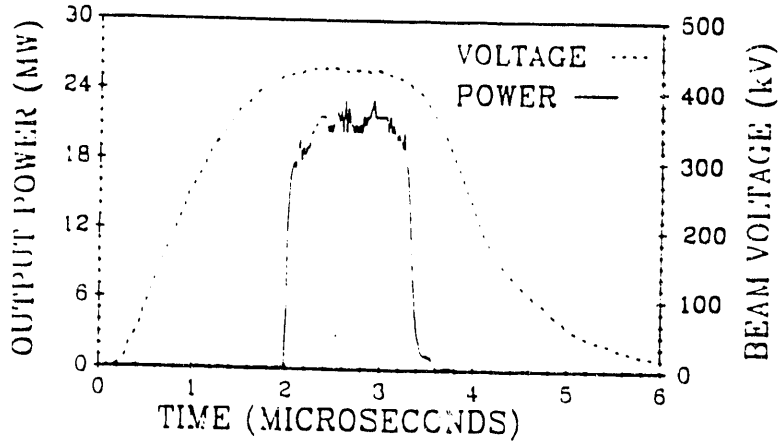

Figure 6. Time dependence of the output power and the beam voltage at the maximum efficiency point.

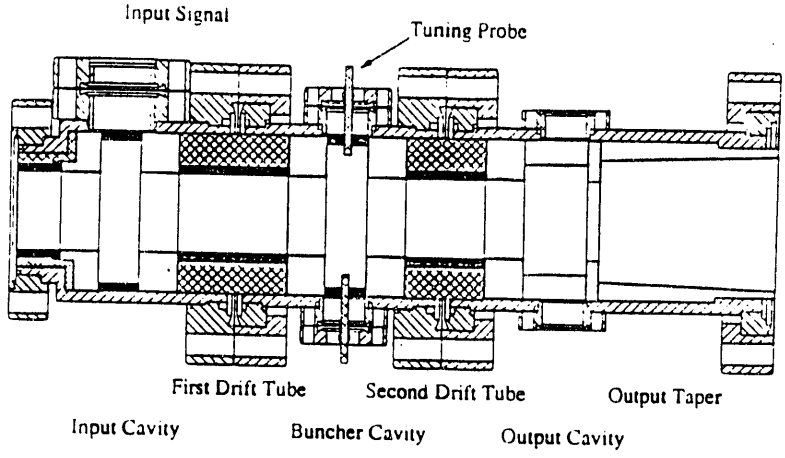

Figure 7. The three-cavity microwave circuit configuration.

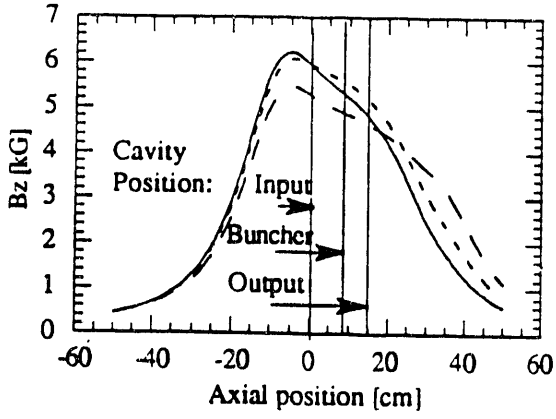

Figure 8. Axial variation of the guide field for the steep and weak tapers used in Tubes 8 and 9. Solid line —— steep taper (30%), broken line - - - weak taper (17%) Tube 8, dotted line - - - - - weak taper (22%) Tube 9.

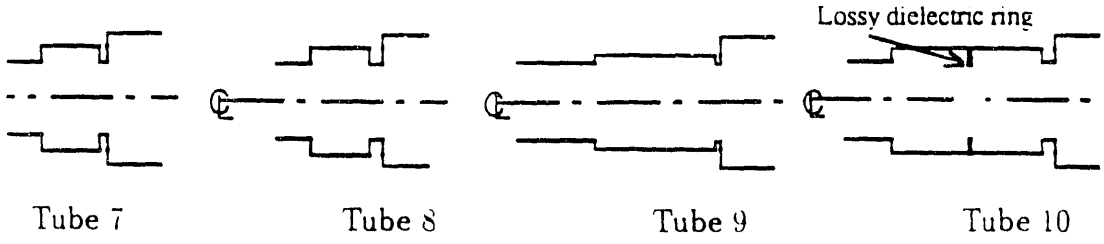

Figure 9. Cross-sectional diagrams of the output cavities of Tubes 7-10.

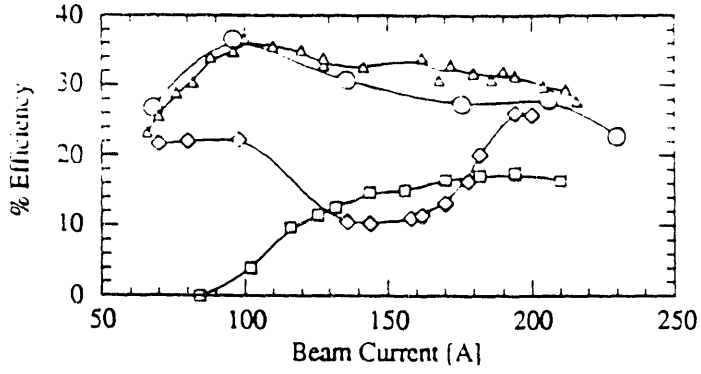

Figure 10. Dependence of efficiency on beam current for Tubes 7-10, at beam voltage 425 kV. The lines with circles (◯) represent Tube 7, triangles (△) Tube 8, diamonds (◇) Tube 9, and squares (□) Tube 10.

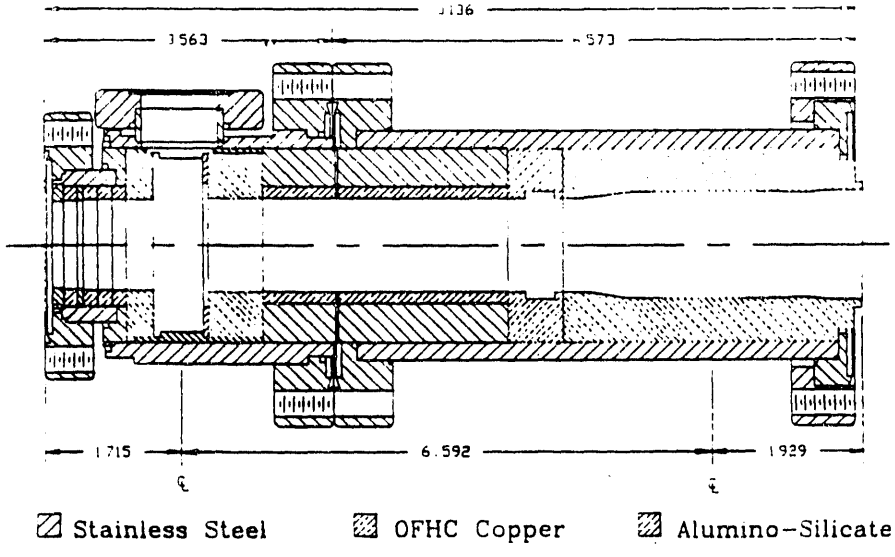

Figure 11. A second harmonic circuit.

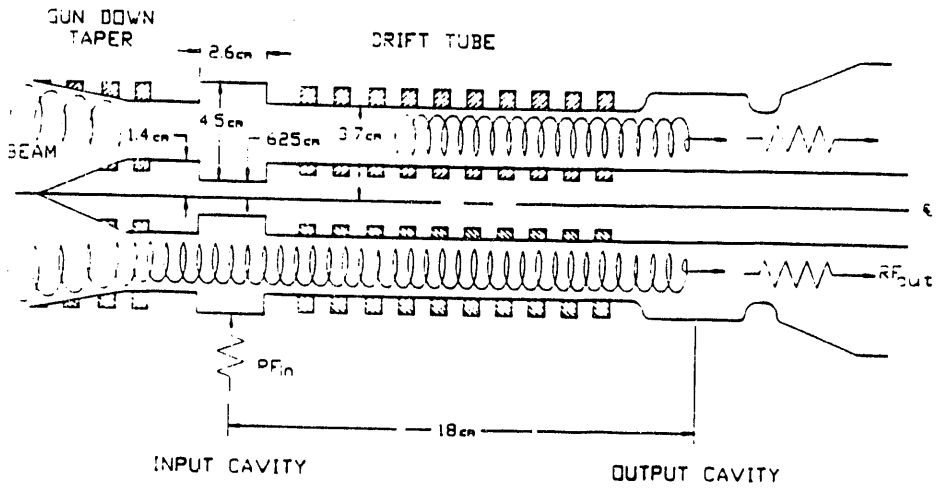

Figure 12. A coaxial second harmonic two-cavity circuit.

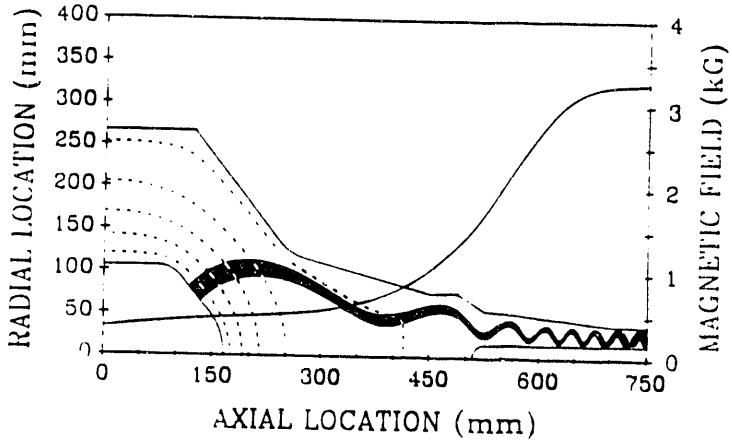

Figure 13. Electrode design and ray trajectories for the 300 MW MIG.

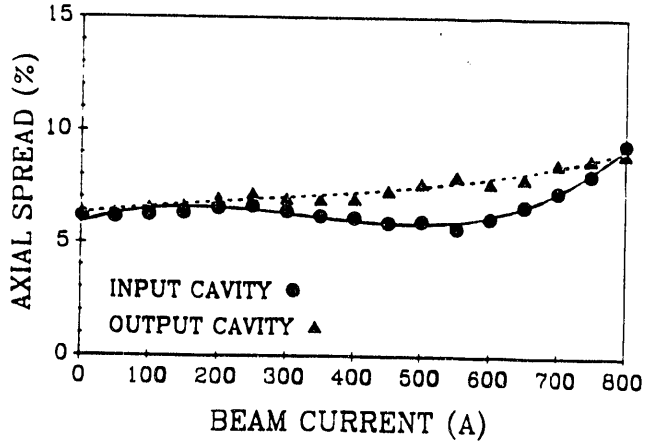

Figure 14. The dependence of axial velocity spread on current.

END

DATE
FILMED
6/22/93